

LETTER TO THE EDITOR

Unidentified emission features in the R Coronae Borealis star V854 Centauri

L. C. Oostrum^{1,2}, B. B. Ochsendorf³, L. Kaper¹, and A. G. G. M. Tielens⁴

¹ Anton Pannekoek Institute for Astronomy, University of Amsterdam, PO Box 94249, 1090 GE, Amsterdam, The Netherlands
e-mail: l.c.oostrum@uva.nl

² ASTRON, The Netherlands Institute for Radio Astronomy, PO box 2, 7990 AA Dwingeloo, The Netherlands

³ Department of Physics and Astronomy, The Johns Hopkins University, 3400 North Charles Street, Baltimore, MD 21218, USA

⁴ Leiden Observatory, Leiden University, PO Box 9513, 2300 RA Leiden, The Netherlands

Received date / Accepted date

ABSTRACT

During its 2012 decline the R Coronae Borealis star (RCB) V854 Cen was spectroscopically monitored with X-shooter on the ESO *Very Large Telescope*. The obscured optical and near-infrared spectrum exhibits many narrow and several broad emission features, as previously observed. The envelope is spatially resolved along the slit and allows for a detailed study of the circumstellar material. In this *Letter* we report on the properties of a number of unidentified emission features (UFs), including the detection of a new one at 8692 Å. These UFs have been observed in the Red Rectangle, but their chemical and physical nature is still a mystery. The previously known UFs behave similarly in the Red Rectangle and V854 Cen, but are not detected in six other observed RCBs. Possibly the presence of some hydrogen is required for the formation of their carrier(s). The 8692 Å UF is present in all RCBs. Its carrier is likely of a carbonaceous molecular nature, presumably different from that of the other UFs.

Key words. circumstellar matter – stars: individual: V854 Cen

1. Introduction

R Coronae Borealis stars (RCBs) are rare, hydrogen deficient supergiants that exhibit strong declines in their brightness (Clayton 2012). Only about a hundred RCBs are known in the Galaxy. Their rarity is an indication of a short evolutionary phase and/or points to a peculiar mode of stellar evolution: (i) a merger between a CO and He white dwarf or (ii) a final helium-shell flash leading to the expansion to supergiant size (Iben et al. 1996; Saio & Jeffery 2002). The decline is thought to be due to the formation of clouds of carbon dust along the line of sight, obscuring the stellar photosphere so that the circumstellar envelope becomes observable in emission. Such a natural coronagraph provides a unique opportunity to study the chemical and physical nature of the circumstellar envelope of these peculiar objects.

Due to the irregularity of these events, limited spectra are available of RCBs in decline. V854 Cen is an RCB that is of particular interest because it is one of the few RCBs that include hydrogen lines in their spectra; It is the most hydrogen-rich RCB after DY Cen (Asplund et al. 1998; Jeffery & Heber 1993). V854 Cen and DY Cen are also the only RCBs in which polycyclic aromatic hydrocarbons (PAHs) have been detected (García-Hernández et al. 2011a). The spectra include the weak 18.9 μm band that is now generally attributed to C₆₀ (Cami et al. 2010; Sellgren et al. 2010). Besides that, V854 Cen shows some unidentified visual emission features (UFs) in its decline spectrum (Rao & Lambert 1993b). These features have only been detected in the Red Rectangle proto-planetary nebula (Schmidt & Witt 1991). In that object, the features change in shape, intensity and peak position as a function of position in the nebula (Van Winckel et al. 2002; Wehres et al. 2011). Additional impetus for

a study of the visual emission features is provided by the potential link between the visual emission bands in the Red Rectangle (RR) and the diffuse interstellar band (DIB) absorption features in the interstellar medium (Sarre et al. 1995).

In this *Letter* we show, for the first time, the spatial structure of the emission features in V854 Cen during its 2012 decline. We compare the characteristics of these features to those detected in the RR. In addition, we search for new emission features (300–2500 nm) in V854 Cen, as well as in six other RCBs.

2. Observations and data reduction

Time on the ESO VLT was granted for observing V854 Cen within a window of four months in 2012. The object was monitored by the American Association of Variable Star Observers (AAVSO). When the star's visual magnitude dropped below $m_v = 8$ (maximum-light $m_v = 7.1$), multiple spectra were obtained with VLT/X-shooter (Vernet et al. 2011) during the decline that lasted around 2.5 months. Additionally, in 2013 X-shooter spectra were taken of V854 Cen and a few other RCBs, known to be in decline as determined from their AAVSO light curves, with the aim to search for the presence of unidentified features. V854 Cen was then at maximum light. For all observations, the highest resolution mode was used, where $R \approx 10000$, 18000, and 11500 for the UVB, VIS, and NIR arms, respectively. A log of observations is given in Table 1.

The spectra were reduced using the X-shooter pipeline version 2.2.0 (Modigliani et al. 2010) and flux calibrated using spectrophotometric standard stars. Telluric correction of the 1D NIR spectra was done with Spextool (Vacca et al. 2003) using telluric standard spectra obtained at similar airmass and close in time to

Table 1. Log of VLT/X-shooter observations. During the rise of V854 Cen, three different position angles were used. The magnitudes were measured from the acquisition images, except for V854 Cen during maximum light, for which they are saturated. For these, values from the AAVSO were used. V854 Cen distance is based on the $(V - I) - M_V$ relation for RCBs in the LMC by Tisserand et al. (2009). For the others, a typical value of $M_V = -5$ (Clayton 2012) is assumed. The signal-to-noise ratio was measured in the continuum around 6200 Å.

Target	d (kpc)	Phase	Obs. date	m_v (max)	m_v (obs)	S/N
V854 Cen	2.4	Max	2012-05-04	7.1 ⁽¹⁾	7.2	90
		Min	2012-06-14		13.3	70
		Min	2012-06-18		12.8	130
		Rise	2012-07-05		9.9	170
		Rise	2012-07-05		9.9	150
		Max	2013-07-15		7.2	85
NSV 8092	17.5	Min	2013-07-15	<11.7 ⁽²⁾	14.0	30
R CrB	1.3	Min	2013-07-15	5.7 ⁽³⁾	13.7	35
RT Nor	9.9	Min	2013-07-15	10.6 ⁽³⁾	15.2	20
RZ Nor	10.5	Min	2013-07-15	10.6 ⁽³⁾	16.2	15
S Aps	7.1	Min	2013-07-15	9.6 ⁽³⁾	14.3	10
V CrA	6.6	Min	2013-07-15	9.4 ⁽³⁾	17.5	10

References. (1) Samus' et al. (2003); (2) Tisserand et al. (2013); (3) Ducati (2002).

the targets. The resulting spectra were shifted to the rest-frame of the observed source.

3. The unidentified emission features

3.1. Detected bands

A section of the X-shooter spectrum of V854 Cen is shown in Fig. 1. The broad features at 5800, 5827, 5854 and 6617 Å were first recognized in V854 Cen by Rao & Lambert (1993b) during a deep decline ($m_V \sim 15$). The similarity between these features and the emission features in the RR was already noted. We expand upon this by considering the spatial and dynamical (i.e. radial velocity) structure of these features in V854 Cen. None of these bands are detected in any of the other observed RCBs. The spectra reveal the presence of a broad emission feature at 8692 Å that has not been seen before in any RCB, nor in the RR.

Of the seven bands, only the $\lambda\lambda$ 5800, 5827, 5854, and 6617 bands are detected in the 2012 decline of V854 Cen. The absence of three of the features (at 5772, 6774 and 6997 Å) may be attributed to the depth of the decline, as this decline is 2 magnitudes – or a factor ~ 6 in flux – shallower than the 1992 decline, and the non-detected features are the weakest ones. The four detected bands are present in the two spectra taken during the deepest part of the decline ($m_V \sim 13$), just beyond the stellar continuum along the slit. The features are strongest in the spectrum taken just after the minimum, on 2012-06-14. Only in that spectrum the S/N in the features is high enough to allow for an analysis of their spatial distribution. The features are detected at different distances from the central object as shown in Fig. 1, which also shows the maximum light spectrum for comparison. The features are only very marginally detected at the Western side of the star (negative offsets), hence we focus on the Eastern side (positive offsets). None of the bands are detected in the other RCBs.

The whole wavelength range of X-shooter (300-2500 nm) has been searched for the presence of emission features. One

new feature was detected, present in *all* V854 Cen spectra, at ~ 8692 Å. It is also detected in five of the six other observed RCBs in decline (Fig. 2). Similar to many features associated with the circumstellar material, this feature is only detected off-source. The feature is blended with two photospheric lines: Sr II λ 8689 and Sc I λ 8694. In order to disentangle the nebular features from the stellar ones, the off-source spectrum is divided by the on-source spectrum and the resulting spectrum renormalised. The presence of the feature during maximum-light is especially noteworthy.

3.2. Spatial and dynamical structure of the bands

As the circumstellar envelope of V854 is spatially resolved along the spectrograph slit, position-velocity (PV) diagrams can be produced to study the kinematic structure of the emission lines as a function of the distance from the star. In Fig. 3 we show the dynamical structure as revealed by the Na I D resonance lines, and UF8692. The other unidentified features are too weak to construct a PV diagram. Both doublet components in Na I D show a structure suggesting that the emission is produced in roughly a shell with a radius of about $3.5''$ and expanding with a velocity of 250 km s^{-1} . The size of the shell is based on the furthest position where the flux is more than 3σ above the noise. PV diagrams of more extended features, confirming the size and velocity of the shell, are shown in Appendix A. The shape of the UF8692 extended emission is different from the shell traced by Na I D. It shows a change in wavelength and width for different distances from the central object. For V854 Cen, it shifts toward the red at the Eastern side of the star (i.e. positive offsets), and to the blue at the Western side of the star. Additionally, it narrows with increasing distance to the star on the Eastern side. It is also worth noting that the equivalent width (W_{eq}) of the feature – here defined such that an emission feature has a positive W_{eq} – increases with distance to the star. This confirms that this newly found feature originates from the circumstellar material.

The behaviour of the λ 8692 feature is different for each RCB. In RT Nor and RZ Nor, the width of the feature does not change significantly, while a narrowing with increasing distance is observed in the others. The position of the feature shifts in all objects. There is no clear pattern to this, in some objects only blueshift is observed, in others also redshift and/or no shift on one side of the star. As the RCBs have different distances, different physical scales are probed, but we do not find a correlation between the behaviour of this feature and the respective distances to the RCBs.

The shape of the bands, when integrated over an interval along the slit, is well described by either one or two Gaussians. All features in the λ 5825 complex are measured together, as those bands are too close in wavelength to be considered separately. For the band at 5800 Å, two Gaussians are used to account for the asymmetric band shape, which significantly improves the fits. For the other bands a single component is used. All sharp emission lines, originating from regions close to the star ($\sim 2R_*$; Clayton 1996) instead of the large-scale circumstellar material, are removed from the spectra prior to the fitting procedure.

For all five detected bands, the measured peak position as function of distance to the star is shown in Fig. 4 (black squares). All features (at $1.6''$ and $2.8''$) are shown in Appendix B. The narrow component in the 5800 Å feature (Fig. 1) is used for the band position, as this component is stronger and dominates the peak position. The same bands in the RR are known to show a blueshift with increasing distance to the central binary sys-

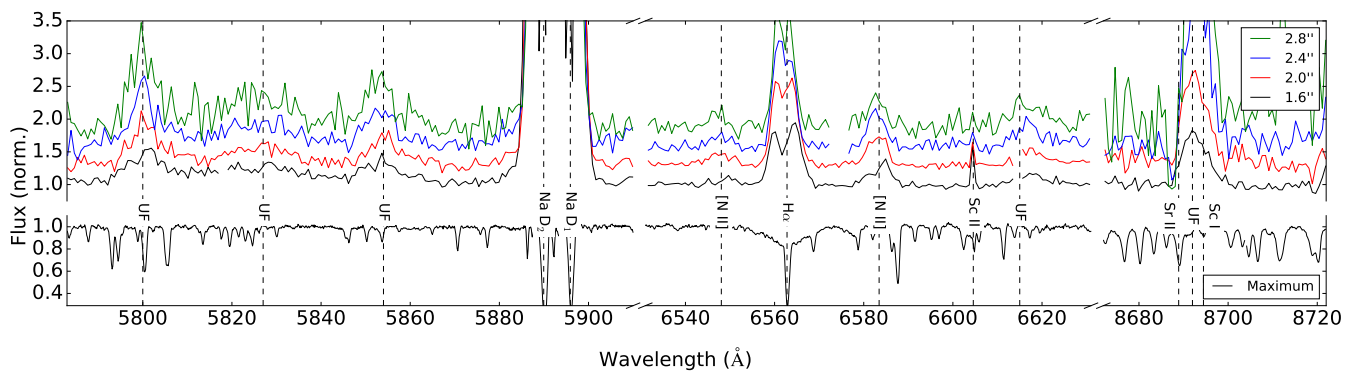


Fig. 1. V854 Cen decline spectra at different offsets from the central object (*see inset*) and at maximum light (*bottom spectrum*). During a decline, the absorption spectrum converts into an emission spectrum, the strongest emission lines being the Na I D doublet. Additionally, a sequence of unidentified emission features (UFs) is clearly detected between 5800 and 5860 Å, at 6617 Å, and at 8692 Å. The narrow Y II λ 6614 emission line has been removed from the 1.6'' and 2.0'' offset spectra for plotting purposes. The absorption lines near 5800 Å and 5854 Å are due to C I and Ba II, respectively.

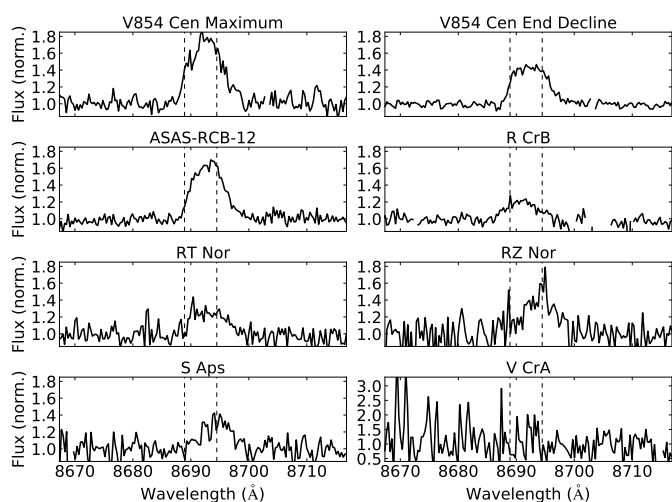


Fig. 2. The λ 8692 UF in all observed RCBs. The two dashed lines indicate the position of the Sr II λ 8689 and Sc I λ 8694 photospheric lines. The UF is detected in all except V CrA. The position and intensity of the feature clearly vary between objects. In V854 Cen the feature is also detected during maximum light.

tem (Van Winckel et al. 2002; Wehres et al. 2011). The same analysis method as for V854 Cen is applied to the RR spectra, except for the number of components: The higher S/N RR spectra require two components for the λ 5854 and λ 6617 bands in addition to λ 5800, whereas one component is sufficient for those bands in V854 Cen. The only RR spectrum covering the λ 8692 feature is from the ESPaDOnS spectrograph mounted on the CFHT, and unfortunately has insufficient signal in that wavelength region (N.L.J. Cox, priv. comm.). The measured RR band positions agree well with those provided by Wehres et al. (2011). With the exception of λ 8692, all V854 Cen and RR bands show a shift towards shorter wavelengths with increasing distance to the central object. The RR bands are clearly shifted towards the blue with respect to V854 Cen, although they are known to be redder than the V854 Cen bands close to the central binary in the RR (Van Winckel et al. 2002). The λ 8692 feature is the only feature detected on both sides of the star, and shows a redshift where the other features show a blueshift.

The RR bands show a correlation between their position and width: Some bands become narrower as they shift to shorter

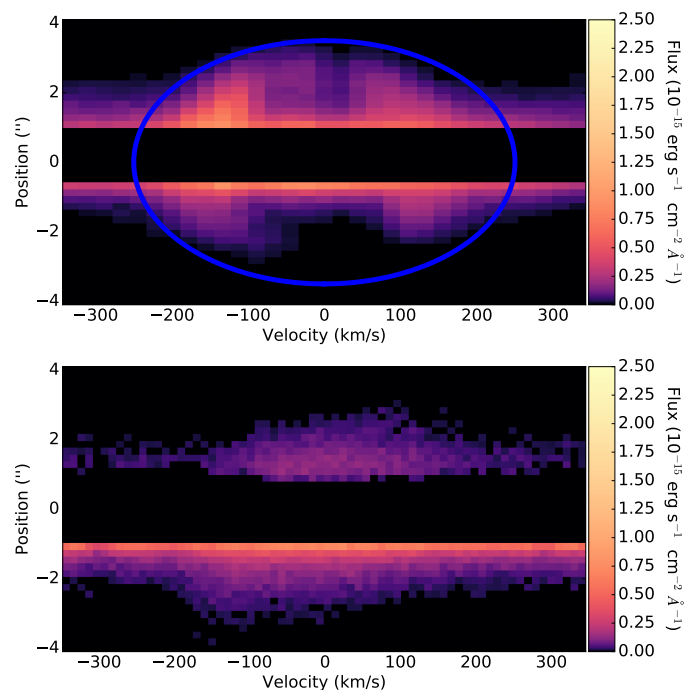


Fig. 3. Position along the spectrograph slit (vertical direction) against radial velocity for the Ca II K resonance line (*top*) and UF at 8692 Å (*bottom*) in V854 Cen. The continuum flux has been subtracted and all flux within 0.7'' of the central object has been set to zero to enhance the visibility of these extended features. The thick blue line shows the expected maximum radial velocity at each position for a spherical shell of radius 3.5'' and expanding with a velocity of 250 km s⁻¹. One sees that the unidentified feature at 8692 Å is spatially extended as well.

wavelengths (Schmidt & Witt 1991; Sarre et al. 1995; Van Winckel et al. 2002; Wehres et al. 2011). We are unable to confirm such a correlation in the V854 Cen features. It should be noted that, in the RR, the features change most rapidly close to the central binary. The distance to V854 Cen is roughly three times that of the RR (710 pc; Men'shchikov et al. 2002). We thus cannot exclude the presence of a width-wavelength correlation in the inner regions of the circumstellar material.

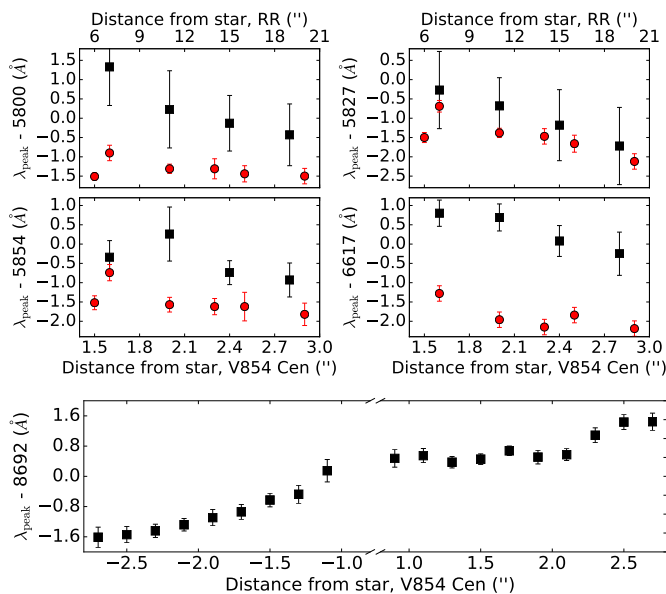


Fig. 4. Band positions of the unidentified features as function of distance to the central object for V854 Cen (black squares) and the Red Rectangle (red circles). There is no measurement of the $\lambda 6617$ feature at $6''$. Error bars reflect 1σ errors. All RR bands are blueshifted with respect to the corresponding bands in V854 Cen. The $\lambda 8692$ band is only covered in V854 Cen and is detected on both sides of the star.

4. Discussion

We detect several emission features in the nebula surrounding V854 Cen, up to $3.5''$ or ~ 8500 AU from the central object. This is the furthest detection of the nebula so far. The broad emission lines from Na I D, H α , and [C I] $\lambda 9850$ show a roughly spherical outflow with velocities up to 250 km s^{-1} . In addition to these atomic lines, we detect six unidentified emission features, including a new one at 8692 \AA . The width of the emission features is comparable to that of other broad emission lines. The UFs that are also detected in the RR have a similar width, even though the velocities in the RR are much lower ($\sim 7 \text{ km s}^{-1}$ in CO; Jura et al. 1995) than in V854 Cen. This indicates that the features are intrinsically broad and hence that their width in V854 Cen is not due to Doppler broadening. The observed shift of $\sim 1 \text{ \AA}$ in the features at $5800 - 5854 \text{ \AA}$ corresponds to $\sim 50 \text{ km s}^{-1}$. This shift may be due to rotational cooling, as in the RR (Wehres et al. 2011), however assuming no cooling it is an upper limit on the radial velocity of the carrier. This velocity is significantly lower than that of the Na I D-traced shell, hence the carriers are not located in that shell. There is, however, evidence for low-velocity dust in RCBs, assuming that the minimum-light optical spectrum is dominated by scattered light from the central object (García-Hernández et al. 2011b). This low-velocity material is the most likely environment for the carrier of the UFs. The absence of the features in other RCBs may indicate that the presence of some hydrogen is required for their formation.

The $\lambda 8692$ feature may provide insight in the geometry of this dust in V854 Cen, as it is the only UF that is detected clearly on both sides of the star. If we interpret the shift in this feature as a Doppler shift, it is consistent with a bipolar outflow which is being accelerated to $\sim 50 \text{ km s}^{-1}$. A bipolar geometry has been suggested in literature (e.g. Rao & Lambert 1993a; Chesneau et al. 2014). If the other UFs are part of the same outflow, we would expect them to show a shift of $\sim 0.3 \text{ \AA}$ between their closest and furthest detection. We are, however, unable to confirm

this, as this putative shift is smaller than the detected shifts in both V854 Cen and the RR. By the same argument as for the other features, the carrier of $\lambda 8692$ is not located in the high-velocity shell.

For the observed bands, the shifts in the RR are consistent with a change in excitation temperature of a molecule (Wehres et al. 2011). For V854 Cen too, one would expect such a shift as the temperature in the outflow decreases.

Care has to be taken when comparing UF8692 to the other features, as it is the only feature present in all spectra and the only one to show up in other RCBs. It is thus unlikely that this feature has the same carrier as one of the other emission bands. The presence of the feature in more hydrogen-deficient RCBs does indicate that the carrier is hydrogen-poor. A carbonaceous molecular nature seems likely, given the high carbon abundances of RCBs. The different behaviour of the feature in different RCBs is quite puzzling. It may be an indication of varying physical and chemical conditions in the complex circumstellar envelopes of RCBs.

It has been suggested that the UFs in the RR are the emission equivalent of the DIBs (e.g. Scarrott et al. 1992). The inverted DIB spectrum does show correlations with some UFs. We are unable to identify a possible DIB counterpart for the $\lambda 8692$ feature. The closest known DIB is located at 8648.3 \AA (online catalogue¹ and N.L.J. Cox, priv. comm.), which is too far off to be the likely absorption equivalent of the $\lambda 8692$ feature.

Acknowledgements. The authors thank Nadine Wehres and Hans van Winckel for providing us the Red Rectangle spectra. We acknowledge the variable star observations from the AAVSO International Database contributed by observers worldwide, and used in this research. LCO would like to thank Nick Cox for discussion about DIBs and the Red Rectangle. LCO acknowledges funding from the European Research Council under the European Union's Seventh Framework Programme (FP/2007-2013) / ERC Grant Agreement n. 617199. Based on observations collected at the European Organisation for Astronomical Research in the Southern Hemisphere under ESO programmes 089.D-0937(A) and 091.C-0934(B).

References

- Asplund, M., Gustafsson, B., Rao, N. K., & Lambert, D. L. 1998, A&A, 332, 651
- Cami, J., Bernard-Salas, J., Peeters, E., & Malek, S. E. 2010, Science, 329, 1180
- Chesneau, O., Millour, F., De Marco, O., et al. 2014, A&A, 569, L4
- Clayton, G. C. 1996, PASP, 108, 225
- Clayton, G. C. 2012, Journal of the American Association of Variable Star Observers (JAAVSO), 40, 539
- Ducati, J. R. 2002, VizieR Online Data Catalog, 2237
- García-Hernández, D. A., Kameswara Rao, N., & Lambert, D. L. 2011a, ApJ, 729, 126
- García-Hernández, D. A., Rao, N. K., & Lambert, D. L. 2011b, ApJ, 739, 37
- Iben, Jr., I., Tutukov, A. V., & Yungelson, L. R. 1996, ApJ, 456, 750
- Jeffery, C. S. & Heber, U. 1993, A&A, 270, 167
- Jura, M., Balm, S. P., & Kahane, C. 1995, ApJ, 453, 721
- Men'shchikov, A. B., Schertl, D., Tuthill, P. G., Weigelt, G., & Yungelson, L. R. 2002, A&A, 393, 867
- Modigliani, A., Goldoni, P., Royer, F., et al. 2010, in Proc. SPIE, Vol. 7737, Observatory Operations: Strategies, Processes, and Systems III, 773728
- Rao, N. K. & Lambert, D. L. 1993a, AJ, 105, 1915
- Rao, N. K. & Lambert, D. L. 1993b, MNRAS, 263, L27
- Saio, H. & Jeffery, C. S. 2002, MNRAS, 333, 121
- Samus', N. N., Goranskii, V. P., Durevich, O. V., et al. 2003, Astronomy Letters, 29, 468
- Sarre, P. J., Miles, J. R., & Scarrott, S. M. 1995, Science, 269, 674
- Scarrott, S. M., Watkin, S., Miles, J. R., & Sarre, P. J. 1992, MNRAS, 255, 11P
- Schmidt, G. D. & Witt, A. N. 1991, ApJ, 383, 698
- Sellgren, K., Werner, M. W., Ingalls, J. G., et al. 2010, ApJ, 722, L54
- Tisserand, P., Clayton, G. C., Welch, D. L., et al. 2013, A&A, 551, A77
- Tisserand, P., Wood, P. R., Marquette, J. B., et al. 2009, A&A, 501, 985
- Vacca, W. D., Cushing, M. C., & Rayner, J. T. 2003, PASP, 115, 389
- Van Winckel, H., Cohen, M., & Gull, T. R. 2002, A&A, 390, 147
- Vernet, J., Dekker, H., D'Odorico, S., et al. 2011, A&A, 536, A105
- Wehres, N., Linnartz, H., van Winckel, H., & Tielens, A. G. G. M. 2011, A&A, 533, A28

¹ <http://leonid.arc.nasa.gov/DIBCatalog.html>

Appendix A: Position-velocity diagrams

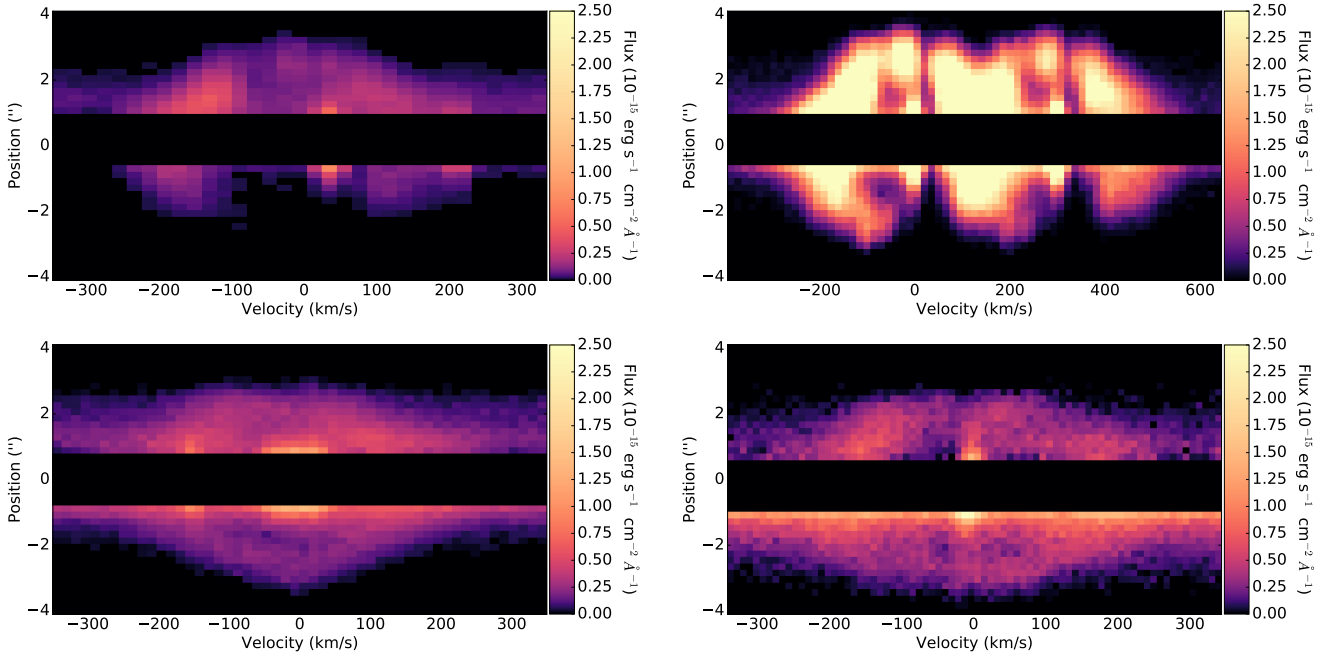


Fig. A.1. Position-velocity diagrams of CH^+ (top left), Na I D (top right), $\text{H}\alpha$ (bottom left) and the $[\text{C I}]$ line at 9850 \AA (bottom right) in V854 Cen. Both CH^+ and Na I D show a shape very similar to Ca II K (see main text); However, both Na I D components have a strong zero-velocity component. Note that the narrow emission line in the CH^+ diagram at $\sim 50 \text{ km s}^{-1}$ is likely due to Na II . $\text{H}\alpha$ and $[\text{C I}]$ show similar, though less pronounced behaviour.

Appendix B: Unidentified feature spectra

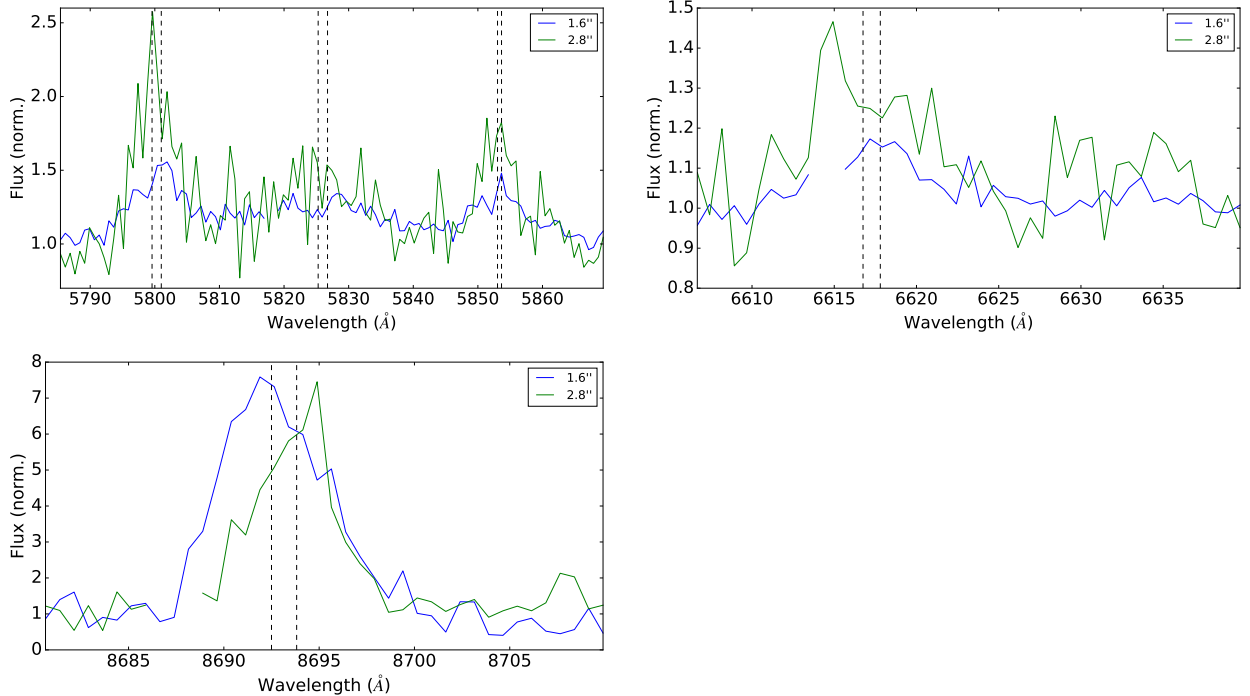


Fig. B.1. Spectra at $1.6''$ and $2.4''$ from the central object for all unidentified features. Dashed lines indicate the best-fit peak position for each feature. *Top left:* $\lambda\lambda 5800, 5827,$ and 5854 . *Top right:* $\lambda 6617$. *Bottom left:* $\lambda 8692$. In all features except $\lambda 8692$, a blueshift with increasing distance from the central object is observed. The $\lambda 8692$ feature shifts toward longer wavelengths in the spectra shown here, but it shifts toward shorter wavelengths on the other side of the star. The $1.6''$ spectrum of $\lambda 8692$ has been stretched by a factor 8 for displaying purposes.